Crystal Structure in Quadrupolar Kondo Candidate PrTr2Al20 (Tr = Ti and V)

doi: 10.7566/JPSJ.88.015001

Crystal structure in quadrupolar Kondo candidate $PrTr_2Al_{20}$ (Tr = Ti and V)

D. Okuyama[1]*, M. Tsujimoto[2], H. Sagayama[3], Y. Shimura[2]†, A. Sakai[2], A. Magata[2], S. Nakatsuji[2], T. J. Sato[1]

[1]*Institute of Multidisciplinary Research for Advanced Materials, Tohoku University, Katahira 2-1-1, Sendai 980-8577, Japan*
[2]*Institute for Solid State Physics, University of Tokyo, Kashiwa, Chiba 277-8581, Japan*
[3]*Condensed Matter Research Center and Photon Factory, Institute of Materials Structure Science, High Energy Accelerator Research Organization, Tsukuba 305-0801, Japan*

We have performed the crystal structure analyses of $PrTr_2Al_{20}$ (Tr = Ti and V). From the anisotropic thermal ellipsoids and the temperature dependence of the lattice constant, it is clarified that the thermal vibration predominantly propagates through the Tr-Al framework. Pr-Al cage especially for PrV_2Al_{20} is anisotropically deformed from sphere, which modify the crystalline-electric-field levels of Pr^{3+}. This information would provide a clue to understand the anomalous properties in $PrTr_2Al_{20}$.

Since two channel (quadrupolar) Kondo effect was theoretically predicted in f^2 electron system,[1)] Pr-based compounds have been extensively studied. Non-magnetic $PrTr_2X_{20}$ (Tr = transition metal, X = Al and Zn) are candidates for the quadrupolar Kondo effect.[2,3)] In PrV_2Al_{20}, magnetic susceptibility and electric resistivity show anomalous $\sqrt{T}$ behavior at low temperatures,[2)] which is in good accordance with the theoretical prediction for the two channel Anderson lattice model.[4)] In stark contrast, $PrTi_2Al_{20}$ shows T^2 behavior below $\sim$ 20 K. Possibly related to the difference in the electron transport, they show quite different ordering behavior. $PrTi_2Al_{20}$ shows non-magnetic anomaly at $T \sim 2$ K, and is ascribed to the ferro-quadrupolar order.[2,5–7)] In contrast, PrV_2Al_{20} shows successive non-magnetic anomalies at much lower temperatures around 0.6 K, of which the origin is suggested to be antiferro-quadrupolar type.[2,8)] The crystal-electric-field (CEF) levels of Pr^{3+} in $PrTi_2Al_{20}$ were determined as Γ_3 (quadrupolar- and octapolar-active ground state) - Γ_4 (5.61) - Γ_5 (9.30) - Γ_1 (13.5 meV),[6)] whereas it was not explored in PrV_2Al_{20}. Both of them shows heavy fermion superconductivity below further lower temperatures, T = 50 mK for Tr = V and 200 mK for Ti.[9,10)]

The electron transport is inevitably affected by the underlying crystal structure, and so are the Pr 4f electron wave functions. Hence, detailed knowledge on the crystal structures, in particular on the difference between the two Tr compounds, would provide a clue to understand the difference of the anomalous transport behavior. Having the above in mind, we revisited crystal structure analysis of the $PrTr_2Al_{20}$. From the results, the crystallographic characters will be discussed.

Synchrotron X-ray diffraction experiments were performed using single crystals with diameters of about 30 μm on the BL-8A at Photon Factory in KEK, Japan. The photon energy of the incident X-rays was tuned at 18 keV. X-ray beams were shaped into a square of 200 × 200 μm^2 by a collimator. The intensity data were converted to the $|F|$-tables by using RapidAuto program, Rigaku. We used CrystalStructure program of Rigaku for analyzing the crystal structure from the $|F|$-table.

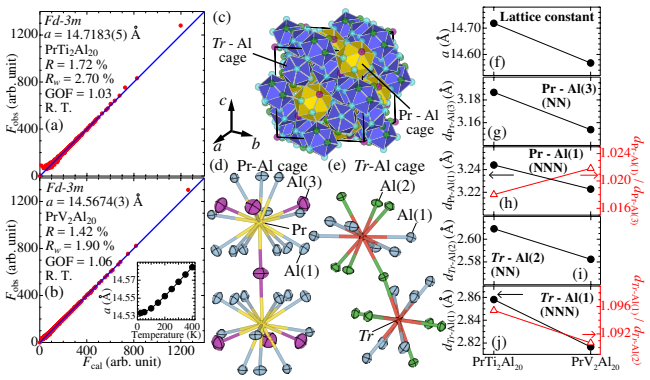

Fig. 1. Comparison between observed (F_{obs}) and calculated (F_{cal}) structure factors for $PrTr_2Al_{20}$ (Tr = Ti (a) and V (b)). (c) Schematic view of crystal structure of $PrTr_2Al_{20}$, Pr-Al cage (d), and Tr-Al cage (e), drawn by VESTA.[21)] Lattice constant (f), nearest neighbor (NN) Pr-Al(3) (g), next-nearest-neighbor (NNN) Pr-Al(1) (h), NN Tr-Al(2) (i), and NNN Tr-Al(1) (j) bond lengths. The (d_{NNN} / d_{NN}) are shown by the open triangular symbol.

We performed crystal structure analyses for single crystals of $PrTi_2Al_{20}$ and PrV_2Al_{20}. The comparisons between observed and calculated structure factors are shown in Figs. 1(a) and 1(b). The structural parameters are summarized in Table I. Here, we also determined the anisotropic atomic displacement parameters, which are not discussed in the earlier work.[11)] The crystal structure consists of two Al-cages with individually capturing Pr and Tr atoms as shown in Fig. 1(c). Here, we call these cages as Pr-Al and Tr-Al cages as illustrated in Figs. 1(d) and 1(e), respectively. In Pr-Al cage, Pr is coordinated by 4 nearest neighbor (NN) Al(3) and 12 next-nearest-neighbor (NNN) Al(1). In Tr-Al cage, the 6 NN Al(2) and 6 NNN Al(1) form a polyhedron. In PrV_2Al_{20}, tiny vacancy at the Pr site was observed.[11)] Lattice constants at room temperature are a = 14.7183(5) and 14.5674(3) Å for $PrTi_2Al_{20}$ and PrV_2Al_{20}, respectively, consistent with the earlier works.[11,12)]

The atomic displacement parameters are quite anisotropic in $PrTr_2Al_{20}$. In the isostructural CeV_2Al_{20}, the phonon density of states (PDOS) was measured using powder inelastic neutron scattering.[13)] By comparing to the simulated PDOS, the isotropic displacement parameters purely due to the thermal vibrations were estimated as: $B_{iso} \sim 1.2$ [Al(3)], 0.68 [Al(1)], 0.52 [Al(2)], 0.44 [Ce], and 0.32 [V]. They are almost identical with the equivalent isotropic displacement parameters of $PrTr_2Al_{20}$ determined in the present study. This strongly suggests that the atomic displacement parameters deduced in the present analysis dominantly represent amplitudes of thermal vibration, and thus the atomic density ellipsoids shown in Figs. 1(d) and 1(e) are indeed thermal ellipsoids. The thermal ellipsoids of Al atoms surrounding Tr or Pr atom spread in the plane perpendicular to the line connecting Al to the central Tr or Pr site. This result indicates the existence of the strong bonding of Tr-Al and/or Pr-Al. Temperature dependence of the lattice constant for PrV_2Al_{20} is shown in the inset of Fig 1 (b). The linear-thermal-expansion coefficient α is $\sim 3 \times 10^{-6}$ (25 K) and $\sim 1.3 \times 10^{-5}$ K^{-1} (150 K), which are quite similar with those for $VAl_{10.1}$,[14)] which has a structure made of only Al-Tr cage part by removing Pr atoms from

*okudaisu@tohoku.ac.jp
†Present address: Graduate School of Advanced Sciences of Matter, Hiroshima University, Higashi-Hiroshima, 739-8530, Japan

Table I. Structure parameters of $PrTr_2Al_{20}$ (Tr = Ti, V) at room temperature. The 7788 and 10541 reflections were observed, and 1576 and 1581 of them are independent for Tr = Ti and V, respectively. The 19 variables were used for the refinement. x, y, and z are the fractional coordinates. *occupancy*, B_{eq}, U_{11}, U_{22}, U_{33}, U_{12}, U_{13}, and U_{23} stand for the site occupancy, equivalent isotropic displacement parameter, and anisotropic displacement parameters.

$PrTi_2Al_{20}$	x and y	z	*occupancy*	B_{eq} (Å^2)	U_{11} and U_{22} (Å^2)	U_{33} (Å^2)	U_{12} (Å^2)	U_{13} (Å^2)	U_{23} (Å^2)
Pr (8*a*)	1/8	1/8	0.999(5)	0.504(3)	0.00638(7)	0.00638(7)	0	0	0
Ti (16*d*)	1/2	1/2	1.010(6)	0.289(4)	0.00366(10)	0.00366(10)	-0.00044(8)	-0.00044(8)	-0.00044(8)
Al1 (96*g*)	0.05939(3)	0.32492(4)	1	0.721(7)	0.01049(16)	0.0064(2)	-0.00359(16)	-0.00022(10)	-0.00022(10)
Al2 (48*f*)	1/8	0.48682(6)	1	0.572(8)	0.00713(17)	0.0075(3)	-0.0027(3)	0	0
Al3 (16*c*)	0	0	1	1.40(2)	0.0177(4)	0.0177(4)	-0.0040(4)	-0.0040(4)	-0.0040(4)
PrV_2Al_{20}									
Pr (8*a*)	1/8	1/8	0.958(3)	0.5472(12)	0.00693(3)	0.00693(3)	0	0	0
V (16*d*)	1/2	1/2	1.007(3)	0.3269(16)	0.00414(4)	0.00414(4)	-0.00045(3)	-0.00045(3)	-0.00045(3)
Al1 (96*g*)	0.058950(10)	0.32555(2)	1	0.719(3)	0.01028(7)	0.00678(8)	-0.00351(7)	-0.00029(4)	-0.00029(4)
Al2 (48*f*)	1/8	0.48679(3)	1	0.537(3)	0.00668(7)	0.00705(10)	-0.00240(9)	0	0
Al3 (16*c*)	0	0	1	1.375(6)	0.01741(15)	0.01741(15)	-0.00366(15)	-0.00366(15)	-0.00366(15)

the $PrTr_2Al_{20}$ structure. This suggests that the lattice vibration is dominated by the framework made of Tr-Al bonds. Therefore, we speculate that the bonds between Tr and Al are dominant, and those for Al and Pr are only weakly connected. It may be noted that the off-diagonal anisotropic displacement parameters in Al sites are unusually large $U_{ij} \sim U_{ii}/3$ ($i \neq j$), compared to those of Tr. They are much larger than those of the other cage compounds, such as clathrates $U_{ij} \sim U_{ii}/10$.[15)]

To investigate the effect of the crystal structure on the CEF of $PrTr_2Al_{20}$ (Pr^{3+} ion under the point symmetry T_d), the lattice constant and bond lengths are summarized in Figs. 1(f) - 1(j). The NNN Pr-Al(1) and Tr-Al(1) bond lengths (d_{NNN}) normalized by the NN Pr-Al(3) and Tr-Al(2) bond lengths (d_{NN}) are also shown, to explain the distortion anisotropy. The lattice constant and bond lengths decreases as Tr changes from Ti to V. In stark contrast, the (d_{NNN} / d_{NN}) for Pr-Al increases as Tr changes from Ti to V. This indicates the Pr-Al cage of PrV_2Al_{20} are much anisotropically deformed from the sphere Al cage. The CEF x and W parameters were known as x = 0.25(1) and W = -1.53(3) K for $PrTi_2Al_{20}$ from the neutron inelastic scattering.[6)] Using the point charge calculation including NN- and NNN-Al sites based on the refined structural parameters of Tr = Ti, we refined the Al-charges to reproduce the x and W parameters obtained in the neutron inelastic experiment.[16–18)] Accordingly, the Al-charges are estimated as +0.9 for Al(1) and +0.88 for Al(3). Next, when we assume Al-charges estimated at Tr = Ti are also applied to Tr = V, we obtained $x \sim 0.41$ and $W \sim$ -2.1 K using the point charge model based on the refined structural parameters for Tr = V. By these parameters, the CEF excited levels can be estimated as $\Gamma_4 \sim 5.6$, $\Gamma_5 \sim 11.1$, and $\Gamma_1 \sim 13.5$ meV for PrV_2Al_{20}. Although the point-charge calculation is known to be crude approximation in intermetallic compounds, the obtained charge values (0.9 and 0.88) are not so far from those for Al in RPd_5Al_2 (R = rare earth).[19)] We also would like to point out that the first excited state in the inelastic neutron scattering was observed around 5 meV in the PrV_2Al_{20},[20)] which is also consistent with the point-charge estimation.

In summary, we performed single-crystal X-ray diffraction to study the crystal structures of $PrTi_2Al_{20}$ and PrV_2Al_{20}. The anisotropic thermal ellipsoids of Al and temperature dependence of lattice constant show that the thermal vibration is dominated by the Tr-Al framework. With increasing the anistropic distorted Pr-Al cage, the Γ_5 CEF-excited energy is particularly enlarged. By the crystal structure and the first principle band calculation, the origin of the anomalous transport properties in $PrTr_2Al_{20}$ should be discussed in the future.

Acknowledgment The authors thank T. Matsumura, Y. Nambu, K. Yamauchi and T. Oguchi for the fruitful discussions. This work was in part supported by partially supported by CREST (JPMJCR15Q5), JST, by KAKENHI (No. 15H05882, 15H05883, 16H02209, 17K14327, 17K18744, and 26103002), MEXT, and by CORE lab of "Five-star Alliance" in "NJRC Mater. & Dev.". The synchrotron X-ray diffraction was performed with the approval of the PF Program Advisory Committee (No.2016G143).

1) D. L. Cox, Phys. Rev. Lett. **59**, 1240 (1987).
2) A. Sakai and S. Nakatsuji, J. Phys. Soc. Jpn. **80**, 063701 (2011).
3) T. Onimaru, K. T. Matsumoto, Y. F. Inoue, K. Umeo, T. Sakakibara, Y. Karaki, M. Kubota, and T. Takabatake, Phys. Rev. Lett. **106**, 177001 (2011).
4) A. Tsuruta and K. Miyake, J. Phys. Soc. Jpn. **84**, 114714 (2015).
5) M. Koseki, Y. Nakanishi, K. Deto, G. Koseki, R. Kashiwazaki, F. Shichinomiya, M. Nakamura, M. Yoshizawa, A. Sakai, and S. Nakatsuji, J. Phys. Soc. Jpn. **80** SA049 (2011).
6) T. J. Sato, S. Ibuka, Y. Nambu, T. Yamazaki, T. Hong, A. Sakai, and S. Nakatsuji, Phys. Rev. B **86**, 184419 (2012).
7) T. Taniguchi, M. Yoshida, H. Takeda, M. Takigawa, M. Tsujimoto, A. Sakai, Y. Matsumoto, and S. Nakatsuji, J. Phys. Soc. Jpn. **85** 113703 (2016).
8) Y. Nakanishi, M. Taniguchi, M. M. Nakamura, J. Hasegawa, R. Ohyama, M. Nakamura, M. Yoshizawa, M. Tsujimoto, S. Nakatsuji, Physica B **536** 125 (2018).
9) A. Sakai, K. Kuga, and S. Nakatsuji, J. Phys. Soc. Jpn. **81**, 083702 (2012).
10) M. Tsujimoto, Y. Matsumoto, T. Tomita, A. Sakai, and S. Nakatsuji, Phys. Rev. Lett. **113**, 267001 (2014).
11) M. J. Kangas, D. C. Schmitt, A. Sakai, S. Nakatsuji, J. Y. Chan, J. Solid State Chem. **196**, 274 (2012).
12) T. Onimaru and H. Kusunose, J. Phys. Soc. Jpn. **85**, 082002 (2016).
13) M. M. Koza, A. Leithe-Jasper, E. Sischka, W. Schnelle, H. Borrmann, H. Mutka, and Y. Grin, Phys. Chem. Chem. Phys. **16**, 27119 (2014).
14) D. J. Safarik, T. Klimczuk, A. Llobet, D. D. Byler, J. C. Lashley, J. R. O'Brien, and N. R. Dilley, Phys. Rev. B **85**, 014103 (2012).
15) A. Bentien, E. Nishibori, S. Paschen, and B. B. Iversen, Phys. Rev. B **71**, 144107 (2005).
16) K. R. Lea, M. J. M. Leask, and W. P. Wolf, J. Phys. Chem. Solids **23**, 1381 (1962).
17) E. Belin-Ferré, *Properties and Applications of Complex Intermetallics* (World Scientific, Singapore, 2009).
18) T. Matsumura, private communication.
19) N. Metoki, H. Yamauchi, H. S. Suzuki, H. Kitazawa, M. Hagihara, T. Masuda, A. A. Aczel, S. Chi, T. Hong, M. Matsuda, D. Pajerowski, and

J. A. Fernandez-Baca, J. Phys. Soc. Jpn. **87**, 094704 (2018).
20) D. Okuyama *et al*. (in preparation).
21) K. Momma and F. Izumi, J. Appl. Crystallogr. **44**, 1272 (2011).